

SHARC-2 350 μ m OBSERVATIONS OF DISTANT SUBMILLIMETER SELECTED GALAXIES

A. KOVÁCS¹, S. C. CHAPMAN¹, C. D. DOWELL¹, A. W. BLAIN¹, R. J. IVISON², I. SMAIL³, AND T.G. PHILLIPS¹

Received 2006 January 26; Accepted 2006 April 27

ABSTRACT

We present 350 μ m observations of 15 Chapman et al. submillimeter galaxies (SMGs) with radio counterparts and optical redshifts. We detect 12 and obtain sensitive upper limits for three, providing direct, precise measurements of their far-infrared luminosities and characteristic dust temperatures. With these, we verify the linear radio–far-infrared correlation at redshifts of $z \sim 1$ –3 and luminosities of 10^{11} – $10^{13} L_{\odot}$, with a power-law index of 1.02 ± 0.12 and rms scatter of 0.12 dex. However, either the correlation constant q or the dust emissivity index β is lower than measured locally. The best fitting $q \simeq 2.14$ is consistent with SMGs being predominantly starburst galaxies, without significant AGN contribution, at far-infrared wavelengths. Gas-to-dust mass ratios are estimated at $54^{+14}_{-11} (\kappa_{850 \mu\text{m}}/0.15 \text{ m}^2 \text{ kg}^{-1})$, depending on the absorption efficiency κ_{ν} , with intrinsic dispersion $\simeq 40\%$ around the mean value. Dust temperatures consistent with $34.6 \pm 3 \text{ K} (\beta/1.5)^{-0.71}$, at $z \sim 1.5$ –3.5, suggest that far-infrared photometric redshifts may be viable, and perhaps accurate to $10\% \lesssim dz/(1+z)$, for up to 80% of the SMG population in this range, if the above temperature characterizes the full range of SMGs. However, observed temperature evolution of $T_d \propto (1+z)$ is also plausible and could result from selection effects. From the observed luminosity-temperature (L - T) relation, $L \propto T_{\text{obs}}^{2.82 \pm 0.29}$, we derive scaling relations for dust mass versus dust temperature, and we identify expressions to inter-relate the observed quantities. These suggest that measurements at a single wavelength, in the far-infrared, submillimeter or radio wave bands, might constrain dust temperatures and far-infrared luminosities for most SMGs with redshifts at $z \sim 0.5$ –4.

Subject headings: galaxies: evolution — galaxies: high-redshift — galaxies: ISM — galaxies: photometry — galaxies: starburst — infrared: galaxies — submillimeter

1. INTRODUCTION

Ever since the first submillimeter-selected galaxy (SMG) samples debuted from SCUBA 850 μ m surveys (Smail et al. 1997; Barger et al. 1998; Hughes et al. 1998; Eales et al. 1999), the nature of the SMG population has been the focus of attention for the galaxy formation community, because the 850 μ m selection is expected to pick similar sources almost independently of redshift ($z \sim 1$ –8), due to a negative K -correction that essentially compensates for the loss of flux from increasing distance. This allows unbiased, luminosity-selected studies of galaxy formation. The hunger for information on these sources spurred a flurry of follow-up studies at all wavelengths, long and short. Since then many of these sources have been identified at optical, UV (Borys et al. 2003; Chapman et al. 2003; Webb et al. 2003) and radio wavelengths (Smail et al. 2000; Ivison et al. 2002), providing accurate positions, which allowed optical redshift measurements (Chapman et al. 2003, 2005). As a result we now know that these massive galaxies, with redshifts distributed around $z \simeq 2.3$, are enshrouded with such quantities of dust that they often lie hidden at optical wavelengths, and therefore constitute a distinct population from the galaxies selected by optical surveys.

More recently, longer wavelength submillimeter surveys, at 1100 and at 1200 μ m (Laurent et al. 2005; Greve et al. 2004), added to the pool of available information. However, the close proximity of the SCUBA, Bolocam, and MAMBO wavelengths on the Rayleigh-Jeans side of the spectral energy distribution (SED) does not allow for an effective con-

straint on the thermal far-infrared spectral SEDs at the relevant redshifts. Nor do the latest results from the *Spitzer Space Telescope* provide powerful constraints, since at the shorter mid-infrared wavelengths the emission is dominated by polycyclic aromatic hydrocarbons (PAHs) and a minority population of hot dust. For these reasons, the best estimates of the characteristic temperatures and the integrated luminosities, to date, have relied on the assumption that the local radio to far-infrared correlation (Helou et al. 1985; Condon 1992; Yun et al. 2001) can be extended into the distant universe. There are hints that this may be appropriate (Garrett 2002; Appleton et al. 2004), but the assumption has remained largely unchecked.

Shorter wavelength submillimeter measurements, sampling near the rest-frame peak of the emission, are thus essential to provide firm constraints to the far-infrared SED. Here we present results at 350 μ m, using the second-generation Submillimeter High Angular Resolution Camera (SHARC-2; Dowell et al. 2003) at the Caltech Submillimeter Observatory (CSO). From these we derive the first direct measures of dust temperatures and far-infrared luminosities for a sample of SMGs, testing the radio to far-infrared correlation. We also attempt to constrain dust emission properties and investigate the implications of our findings for the viability of photometric redshifts based on far-infrared and radio measurements. Finally, we present a range of useful scaling relations that may apply to the SMG population.

2. SHARC-2 350 μ m OBSERVATIONS

We conducted follow-up observations of SCUBA 850 μ m detected sources with radio identifications and optical redshifts (Chapman et al. 2003, 2005). Seven of the 15 targets were hand-picked on the basis of their predicted bright 350 μ m fluxes ($S_{350 \mu\text{m}} > 45 \text{ mJy}$ from Chapman et al. 2005), while the remaining were selected at random to partially com-

¹ California Institute of Technology, Mail Code 320-47, 1200 E California Blvd, Pasadena, CA 91125

² Royal Observatory, Blackford Hill, Edinburgh EH9 3HJ, UK

³ Institute for Computational Cosmology, Durham University, South Road, Durham DH1 3LE, UK

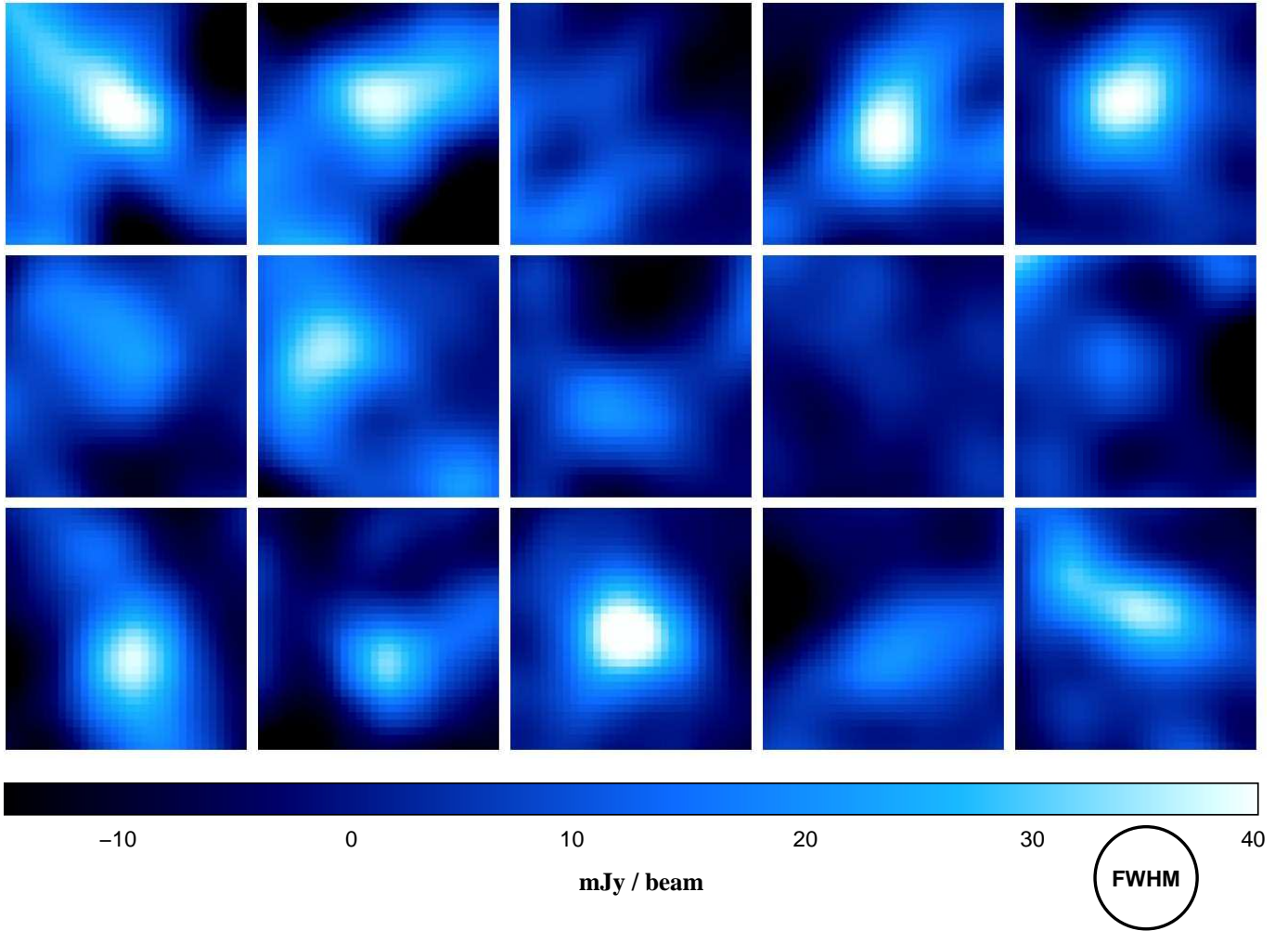


FIG. 1.— $30'' \times 30''$ SHARC-2 $350\mu\text{m}$ thumbnail images of the SMGs observed (sources 1–15 in Tables 1–3) shown in reading order (*left to right, top to bottom*). Images are centered on the radio positions, and displayed on the same flux scale for comparison. The $12''.4$ FWHM effective beams of the optimally filtered (convolved) images are also indicated. Sources 3, 9, and 10 are not detected.

pensate for any selection bias.

The observations were carried out during eight separate observing runs between 2002 November and 2005 April, in excellent weather ($\tau_{225\text{GHz}} < 0.06$), reaching 1σ depths of 5–9 mJy in 2–4 hours of integration in 14 small fields ($\simeq 2.5 \times 1 \text{ arcmin}^2$) around the targeted sources. Our scanning strategy was to modulate the telescope pointing with a small-amplitude ($15''$ – $20''$) nonconnecting Lissajous pattern within the limits of reasonable telescope acceleration (with typical periods of 10–20 s). This pattern was chosen to provide fast, two-dimensional, recurring but non-closed patterns with crossing paths—all of which are essential to allow the separation of the superposed source, atmospheric, and instrumental signals. For the observations since 2003 February, we have taken advantage of the CSO’s Dish Surface Optimization System (Leong 2005) to improve beam shapes and efficiencies, and hence sensitivities, at all elevations.

Pointing corrections were retroactively applied to the observations by a careful fit to the pointing data taken during each run. In addition, our preliminary source identifications revealed a small, albeit significant ($\simeq 3''$) systematic pointing shift in the negative R.A. direction. All maps were realigned accordingly. The reconstructed pointing is accurate to $3''.5$ rms, in good agreement with CSO specifications.

The data were processed using the CRUSH⁴ software package, developed at Caltech (Kovács 2006), which models total power detector signals using an iterated sequence of maximum likelihood estimators. The FWHM point-spread functions of the final maps (Fig. 1) are approximately $12''$ after optimal filtering to search for beam-sized ($\simeq 9''$) features in order to yield maximal signal-to-noise ratios on point sources. This degradation of the image resolution by approximately $\sqrt{2}$, from the nominal instrumental beam width of $8''.5$, is because the fitting for beam-sized features is equivalent to convolving the image with the slightly wider effective beam of around $9''$, which accounts for the smearing of the nominal beam by pointing and focus variations on the long integrations.

Calibration was performed primarily against planets and asteroids, when available, or using stable galactic continuum sources and Arp 220.⁵ Trends in aperture efficiency, especially with elevation, were estimated and were taken into account when calibrating our science targets. The systematic flux filtering effect of the aggressive reduction parameters used in CRUSH to subtract noise signals and reach maximal image depths, was carefully estimated for the case of point

⁴ See <http://www.submm.caltech.edu/sharc/crush>

⁵ See <http://www.submm.caltech.edu/sharc/analysis/calibration.htm>

TABLE 1
SUMMARY OF OBSERVATIONS

ID	Name	Offset ^a (J2000.0) (arcsec)	z	$S(350\mu\text{m})$ (mJy)	$S(850\mu\text{m})$ (mJy)	$S(1100\mu\text{m})$ (mJy)	$S(1200\mu\text{m})$ (mJy)	$S(1.4\text{GHz})$ (μJy)
1	SMM J030227.73+000653.5	+1.0, +0.8	1.408	42.2 ± 9.8	4.4 ± 1.3	217 ± 9
2	SMM J105207.49+571904.0	-1.0, +3.7	2.689	38.0 ± 7.2	6.2 ± 1.6	...	(0.4 ± 0.8)	277.8 ± 11.9
3 ^b	SMM J105227.77+572218.2	...	1.956	(11.3 ± 6.7)	7.0 ± 2.1	5.1 ± 1.3 ^b	3.1 ± 0.7	40.4 ± 9.4 ^c
4 ^b	SMM J105230.73+572209.5	+3.3, -1.8	2.611	41.0 ± 6.8	11.0 ± 2.6	5.1 ± 1.3 ^b	2.9 ± 0.7	86.3 ± 15.4 ^c
5	SMM J105238.30+572435.8	+1.4, +2.5	3.036	40.5 ± 6.5	10.9 ± 2.4	4.8 ± 1.3	4.8 ± 0.6	61.0 ± 22.0 ^c
6	SMM J123600.15+621047.2	-1.4, +2.0	1.994	22.3 ± 6.3	7.9 ± 2.4	131 ± 10.6
7	SMM J123606.85+621021.4	+6.7, +3.5	2.509	35.1 ± 6.9	11.6 ± 3.5	74.4 ± 4.1
8	SMM J131201.17+424208.1	...	3.405	21.1 ± 7.7	6.2 ± 1.2	49.1 ± 6.0
9	SMM J131212.69+424422.5	+2.2, -4.2	2.805	(3.7 ± 4.4)	5.6 ± 1.9	102.6 ± 7.4
10	SMM J131225.73+423941.4	...	1.554	(14.7 ± 7.4)	4.1 ± 1.3	752.5 ± 4.2
11	SMM J163631.47+405546.9	-1.3, -4.0	2.283	38.3 ± 5.5	6.3 ± 1.9	...	(1.1 ± 0.7)	99 ± 23
12	SMM J163650.43+405737.5	-1.0, -1.7	2.378	33.0 ± 5.6	8.2 ± 1.7	...	3.1 ± 0.7	221 ± 16
13	SMM J163658.19+410523.8	+1.1, -1.2	2.454	45.2 ± 5.3	10.7 ± 2.0	...	3.4 ± 1.1	92 ± 16
14	SMM J163704.34+410530.3	-1.8, -4.4	0.840	21.0 ± 4.7	11.2 ± 1.6	...	(0.8 ± 1.1)	45 ± 16
15	SMM J163706.51+405313.8	-2.3, +2.4	2.374	36.1 ± 7.7	11.2 ± 2.9	...	4.2 ± 1.1	74 ± 23
(16)	SMM J163639.01+405635.9	...	1.495	...	5.1 ± 1.4	...	3.4 ± 0.7	159 ± 27
(17) ^d	SMM J105201.25+572445.7	...	2.148	24.1 ± 5.5	9.9 ± 2.2	4.4 ± 1.3	3.4 ± 0.6	72.1 ± 10.2
(18)	SMM J105158.02+571800.2	...	2.239	...	7.7 ± 1.7	...	2.9 ± 0.7	98.1 ± 11.6
(19) ^{d,e}	SMM J105200.22+572420.2	...	0.689	15.5 ± 5.5	5.1 ± 1.3	4.0 ± 1.3	2.4 ± 0.6	57.4 ± 13.2
(20) ^d	SMM J105227.58+572512.4	...	2.142	44.0 ± 16.0	4.5 ± 1.3	4.1 ± 1.3	2.8 ± 0.5	39.2 ± 11.4 ^c
(21) ^f	SMM J105155.47+572312.7	...	2.686	...	5.7 ± 1.7	...	3.3 ± 0.8	46.3 ± 10.2

NOTE. — MAMBO 1200 μm fluxes are from Greve et al. (2004), upper limits (bracketed fluxes) are from T. Greve (2006, private communication), Bolocam 1100 μm fluxes are from Laurent et al. (2006), and 850 μm SCUBA and 1.4GHz fluxes are taken from Chapman et al. (2005). Biggs & Ivison (2006) provide alternative radio fluxes for many of the listed objects. The bracketed IDs indicate sources that have not been observed by the authors within the context of this paper, but archived data are used in the analysis.

^aSHARC-2 detection offsets are with respect to the published radio positions.

^bBoth of these sources are likely contributors to the observed 1100 μm flux. The Bolocam data are ignored in the analysis.

^cThe alternative radio fluxes from Biggs & Ivison (2006) are significantly different from or more accurate than the values listed here.

^dSHARC-2 350 μm fluxes from Laurent et al. (2006).

^eChapman et al. (2005): “These SMGs have double radio identifications, one lying at the tabulated redshift and a second lying at $z < 0.5$.” The higher redshift source is assumed to be the dominant contributor.

^fChapman et al. (2005): “These SMGs have double radio identifications, both confirmed to lie at the same redshift.”

sources, and the appropriate corrections were applied to the images. The final calibration is expected with high confidence to be more accurate than 15%, with systematic effects anticipated to be less.

The maps produced by CRUSH reveal Gaussian noise profiles with an anticipated tail at positive fluxes. Hence, in searching for 350 μm counterparts around the published radio positions, we calculate detection thresholds based on the effective number of beams $N_{\text{beam}} \approx 1 + A/A_{\text{beam}}$ (Kovács 2006) inside a detection area A in the smoothed image. A detection confidence $C \approx 1$ is reached at the significance level S/N , at which

$$1 - C \approx \frac{N_{\text{beam}}}{\sqrt{2\pi}} \int_{S/N}^{\infty} e^{-1/2x^2} dx. \quad (1)$$

As for the appropriate search radius, the probability that the peak of the smoothed image falls at some radius away from the true position is essentially the likelihood that the smoothed noise level at that radius is sufficient to make up for the deficit in the underlying signal. Therefore, for the case of Gaussian noise profiles, we expect the detection to lie inside of a 2σ noise peak, and therefore within a maximal radius given by the condition $S/N = 2/[1 - \exp(-r_{\text{max}}^2/2\sigma_{\text{beam}}^2)]$ for a Gaussian beam profile with σ_{beam} spread at an underlying signal-to-noise ratio of S/N . To this we must add the appropriate pointing tolerance (at 2σ level) in quadrature, arriving at an expression for the detection radius around the actual position as a function of detection significance, that is,

$$r_{\text{max}}^2 = 4\sigma_{\text{pointing}}^2 - 2\sigma_{\text{beam}}^2 \ln\left(1 - \frac{2}{S/N}\right). \quad (2)$$

Note that this expression simplifies to $r_{\text{max}} \rightarrow 2\sigma_{\text{beam}}(S/N)^{-1/2}$ for the case of $S/N \gg 1$ and negligible σ_{pointing} .

The combination of $S/N = 2.30$ and $r_{\text{max}} = 10''.4$ simultaneously satisfy both constraints (eqs. [1] and [2]) at $C = 95\%$ confidence level for a $\sigma_{\text{beam}} = 9''$ effective beam and $\sigma_{\text{pointing}} = 3''.5$ pointing rms. Potential candidates thus identified are subsequently verified to lie within the expected distance from their respective radio positions. The resulting identifications are summarized in Table 1. When counterparts were not found, the peak measurement values inside the search area are reported.

The sources, collectively, are much smaller than the SHARC-2 beam (i.e., $d \ll 9''$), as neither (1) fitting larger ($12''$) beams or (2) filtering extended structures produces systematically different fluxes for the sample as a whole. Source extents typically $\lesssim 30\text{kpc}$ are therefore implied. While the partial resolution of a few objects cannot be excluded, the peak fluxes of the optimally filtered images are expected to be generally accurate measures of the total integrated flux for the objects concerned.

3. SPECTRAL ENERGY DISTRIBUTIONS OF SMGs

We fitted the SHARC-2 350 μm and SCUBA 850 μm fluxes, combined with Bolocam 1100 μm (Laurent et al. 2005) and MAMBO 1200 μm (Greve et al. 2004) data when available, with single-temperature, optically thin greybody models of the form $S(\nu, T) \propto \kappa(\nu)B(\nu, T)$, where $\kappa(\nu) \propto \nu^\beta$ is an approximation for the full emissivity term $(1 - \exp[(\nu/\nu_0)^\beta])$ for $\nu_{\text{obs}} \ll \nu_0$. Alternative SED models incorporating the full optical depth, or a distribution of temperatures and power-law

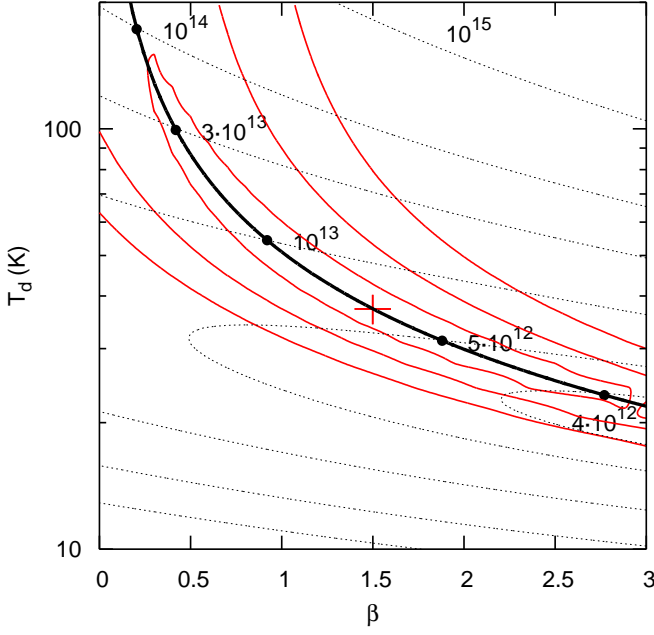


FIG. 2.— Characteristic dust temperature T_d and effective emissivity index β are highly correlated parameters of the SED fit for the typical SMG, even when three photometric data points allow simultaneous fitting of both T_d and β (source 13 from Table 2, shown with solid 1,2 and 3σ contours). However, by assuming $\beta = 1.5$, we can accurately constrain luminosities (dotted contours) and temperatures, which are listed in Tables 2 and 3. The derived properties may be scaled to other β values of the reader's preference using the relations of eq. (3) (thick solid line).

Wien tails, did not provide a better description of the data. Specifically, the flattening of the Rayleigh-Jeans slope due to optical depths approaching unity is not detectable with the $\simeq 10\%$ uncertain relative calibration of the bands, while the Wien side of the spectra is not sampled by the observations. More complex SED models, e.g. the two-temperature model used by Dunne & Eales (2001), were not considered, since these require a greater number of parameters than can be determined from the few, often just two, photometric data points available for the typical SMG.

SED models, whether incorporating an emissivity slope, full optical depth or multiple temperature components, are simple parametrizations of complex underlying spectral distributions, produced by a range of dust properties inside the targeted galaxies. Therefore, T and β of the model describe not the physical temperature and emissivity of every single dust grain, but provide an effective characterization of dust emission in a galaxy as a whole. In this sense, the characteristic β -values, expected in the range 1–2, reflect both the underlying grain emissivities and a distribution of physical temperatures within the observed objects. The derived T -values provide an effective comparison of the characteristic dust temperatures among objects with equivalent SED parametrization.

Simultaneous fitting of T and β requires at least three photometric data points (while many SMGs have only two), and even when permitted these are highly correlated parameters of the fit for the typical SMG (Fig. 2). Therefore, we initially assume $\beta = 1.5$ for the SED fit, as it provides good characterization of actively star-forming environments, both in accurately modeled Galactic clouds (Dupac et al. 2003) and galaxies of the local universe (Dunne & Eales 2001), and is broadly consistent with laboratory measurements on carbide and silicate grains (Agladze et al. 1996). The properties, thus derived, may be scaled to the β -values of the reader's choosing, via

TABLE 2
FAR-INFRARED PROPERTIES OF SMGS FROM SHARC-2 DATA

ID	T_d (K)	$\log L_{FIR}$ (L_\odot)	q_L	ϵ	λ
1	43.3 ± 18.7	12.83 ± 0.64	2.39 ± 0.64	1.36	2.94
2	66.8 ± 26.1	13.49 ± 0.57	2.31 ± 0.57	1.61	3.69
3	21.3 ± 3.8	11.95 ± 0.24	1.91 ± 0.26	0.50	0.21
4	40.1 ± 5.8	12.98 ± 0.19	2.33 ± 0.21	0.84	1.06
5	39.1 ± 4.2	13.03 ± 0.14	2.39 ± 0.21	0.69	0.66
6	25.7 ± 4.7	12.28 ± 0.18	1.71 ± 0.18	0.52	0.35
7	31.0 ± 5.3	12.73 ± 0.15	2.19 ± 0.15	0.54	0.39
8	40.9 ± 8.2	12.85 ± 0.25	2.20 ± 0.26	0.57	0.46
9	21.1 ± 6.3	11.95 ± 0.29	1.16 ± 0.29	0.31	0.04
10	24.3 ± 6.8	11.88 ± 0.35	0.79 ± 0.35	0.59	0.50
11	53.4 ± 16.2	13.18 ± 0.42	2.61 ± 0.43	1.38	2.88
12	34.5 ± 4.5	12.72 ± 0.17	1.75 ± 0.17	0.73	0.77
13	37.3 ± 5.0	12.93 ± 0.16	2.31 ± 0.18	0.77	0.91
14	16.8 ± 2.3	11.38 ± 0.15	2.13 ± 0.22	0.65	0.53
15	31.5 ± 4.2	12.71 ± 0.16	2.23 ± 0.21	0.65	0.57
(17)	27.4 ± 3.0	12.41 ± 0.15	2.02 ± 0.16	0.61	0.44
(19)	14.2 ± 2.2	10.97 ± 0.21	1.82 ± 0.23	0.58	0.41
(20)	40.6 ± 12.3	12.87 ± 0.48	2.76 ± 0.50	0.99	1.61

NOTE. — A summary of the derived far-infrared properties of the observed SMGs. All quantities were derived using an optically thin approximation with $\beta = 1.5$. Temperatures and luminosities may be scaled to other β -values using the relations of eq. (3) and the corresponding indices ϵ and λ listed here. The q_L values derived from the radio data of Biggs & Ivison (2006) tend to be higher than these by 0.06 on average.

TABLE 3
PROPERTIES OF SMGS INCORPORATING RADIO DATA

ID	T_d (K)	$\log L_{FIR}$ (L_\odot)	$\log M_d$ (M_\odot)	ϵ	λ
1	37.2 ± 3.8	12.60 ± 0.12	8.64 ± 0.17	0.82	1.09
2	60.3 ± 6.1	13.34 ± 0.12	8.22 ± 0.16	0.86	1.15
3	23.5 ± 2.5	12.10 ± 0.15	9.24 ± 0.17	0.72	0.82
4	37.1 ± 3.4	12.86 ± 0.11	8.91 ± 0.14	0.77	0.89
5	36.8 ± 3.3	12.94 ± 0.12	9.01 ± 0.12	0.67	0.65
6	38.6 ± 7.0	12.66 ± 0.13	8.61 ± 0.33	0.94	1.29
7	30.3 ± 3.9	12.71 ± 0.09	9.24 ± 0.25	0.68	0.78
8	39.8 ± 4.5	12.81 ± 0.12	8.69 ± 0.19	0.71	0.93
9 ^a	21.1 ± 6.3	11.95 ± 0.29	9.36 ± 0.48	0.31	0.04
10 ^a	24.3 ± 6.8	11.88 ± 0.35	8.93 ± 0.37	0.59	0.50
11	41.5 ± 4.4	12.82 ± 0.13	8.60 ± 0.16	0.80	0.99
12	43.2 ± 4.7	13.01 ± 0.10	9.69 ± 0.17	0.96	1.40
13	34.8 ± 3.2	12.84 ± 0.10	9.04 ± 0.14	0.73	0.83
14	16.8 ± 1.9	11.38 ± 0.14	9.32 ± 0.19	0.72	0.74
15	30.7 ± 3.2	12.68 ± 0.12	9.18 ± 0.16	0.70	0.75
(17)	28.6 ± 2.3	12.47 ± 0.12	9.14 ± 0.13	0.75	0.85
(19)	16.4 ± 1.7	11.17 ± 0.13	9.17 ± 0.16	0.81	1.02
(20)	28.6 ± 3.5	12.31 ± 0.17	8.98 ± 0.15	0.76	1.02

NOTE. — Quantities were derived similarly to Table 2, except that the radio data are also incorporated with $q_L = 2.14$. The estimate of the dust masses additionally assumes $\kappa_d(850 \mu\text{m}) = 0.15 \text{ m}^2 \text{ kg}^{-1}$ for the dust absorption efficiency.

^aThese SMGs are identified as being radio-loud. Therefore, the radio data are not used in constraining the far-infrared SEDs.

the deduced spectral indices ϵ and λ listed in the Tables 2 and 3, as

$$T_d \propto \beta^{-\epsilon}, L_{FIR} \propto \beta^{-\lambda}, M_d \propto \beta^{\epsilon(4+\beta)-\lambda}. \quad (3)$$

We included 15% calibration uncertainty in addition to the published statistical uncertainties for all submillimeter data. Nevertheless the luminosities are constrained accurately because the SHARC-2 350 μm measurement falls near the emission peak for all of these sources (Fig. 3).

Flux boosting or Eddington bias (Coppin et al. 2005), in the case of less significant detections, where the selection is in

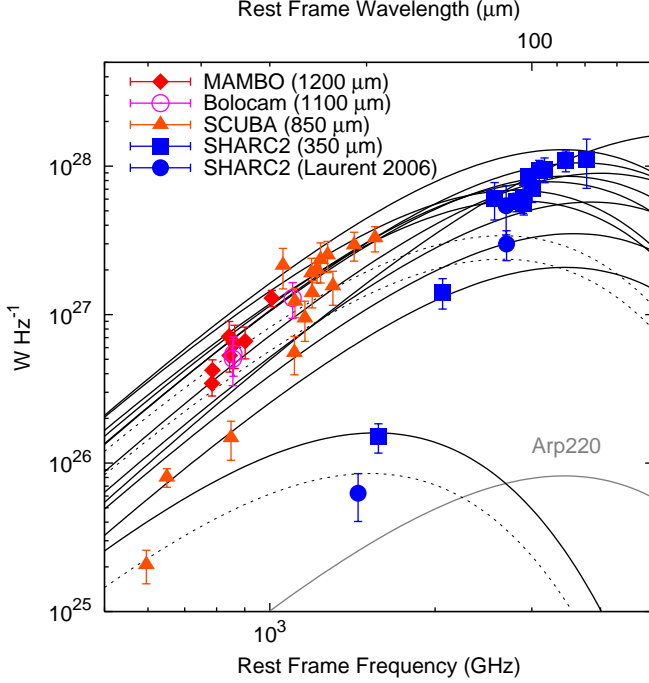


FIG. 3.— Optically thin greybody SED models were fitted (solid lines) to the various available observed fluxes and are transformed to the rest frames of the galaxies for comparison. Fits using (Laurent et al. 2006) data also shown (dashed lines). All the spectra peak in the neighbourhood of the redshifted 350 μm point, providing testimony of the pivotal importance of the SHARC-2 data point in constraining these models. The SEDs shown represent our best fit to the data for sources detected by SHARC-2, use an emissivity index $\beta = 1.5$, and incorporate radio fluxes via the far-infrared to radio correlation with $q_L = 2.14$ with an assumed 0.12 dex dispersion.

the submillimeter, induce a small bias in the derived SEDs. As the bias will not apply to follow-up measurements, and because the exact quantification of the Eddington bias is non-trivial, requiring a-priori knowledge of the underlying source distributions, we left fluxes uncorrected for its effects.

For the first time we are able to use multiband photometry to accurately determine the characteristic dust temperatures and far-infrared luminosities for the SMG population. Luminosities (Tables 2 and 3) are calculated analytically from the fitted grey body model $S(\nu, T)$, following De Breuck et al. (2003):

$$L_{FIR} = 4\pi D_L^2 \Gamma(4+\beta) \zeta(4+\beta) \left(\frac{kT}{h\nu} \right)^{4+\beta} \left(e^{h\nu/kT} - 1 \right) \nu S(\nu, T), \quad (4)$$

where luminosity distances (D_L) were obtained⁶ for a Λ CDM cosmology with $H_0 = 65 \text{ km s}^{-1} \text{ Mpc}^{-1}$, $\Omega_M = 0.3$ and $\Omega_\Lambda = 0.7$. The above expression provides the correct SED integral as long as the transition from the optically thin greybody approximation to optically thick blackbody is above the emission peak where the contribution to the total luminosity is negligible. If power-law Wien tails, with spectral slopes of $-\alpha$ (Blain et al. 2003), are assumed instead, the luminosities can be scaled by a constant $\eta_\beta(\alpha)$, which is around 1.5 for an Arp220 type template with $\alpha = 2$. More generally, in the range of $\alpha \sim 1.1$ –4.0 and $\beta \sim 0$ –3, the values of η are well approximated (with an rms of 5% or 0.02 dex) by the empirical formula

$$\eta_\beta(\alpha) \approx (1.44 + 0.07 \beta)(\alpha - 1.09)^{-0.42}.$$

⁶ See <http://www.astro.ucla.edu/~wright/CosmoCalc.html>

Similar corrections may be derived for the case of increasing optical depth, with η as a function of $h\nu_0/kT$.

Illuminated dust masses (Table 3) were also estimated from the SED model $S(\nu, T)$, using (De Breuck et al. 2003),

$$M_d = \frac{S(\nu, T) D_L^2}{(1+z) \kappa_d(\nu_{\text{rest}}) B(\nu_{\text{rest}}, T_d)}.$$

Here, the normalization for the absorption efficiency was assumed to be $\kappa_{850 \mu\text{m}} = 0.15 \text{ m}^2 \text{ kg}^{-1}$, representing the extrapolated average 125 μm value of $2.64 \pm 0.29 \text{ m}^2 \text{ kg}^{-1}$ (Dunne et al. 2003) from various models by assuming β of 1.5. In comparison to the gas masses derived from⁷ CO measurements (Greve et al. 2005; Tacconi et al. 2006), we find an average gas-to-dust ratio of 54_{-11}^{+14} ($\kappa_{850 \mu\text{m}}/0.15 \text{ m}^2 \text{ kg}^{-1}$), resembling the ratios seen in nuclear regions of local galaxies by Seaquist et al. (2004), who assume a $\kappa_d X_{\text{CO}}$ product comparable to ours. The individual measurements indicate an intrinsic spread of $\simeq 40\%$ around the mean value. The low ratios may be interpreted as an indication for the relative prevalence of dust in SMGs over the local population, which typically exhibit Milky Way like gas-to-dust ratios around 120 (Stevens et al. 2005) or, alternatively, that absorption in SMGs is more efficient with $\kappa_{850 \mu\text{m}} \approx 0.33 \text{ m}^2 \text{ kg}^{-1}$.

Our estimates of the dust temperatures, and hence luminosities, are systematically lower, than those anticipated based on the 850 μm and 1.4 GHz fluxes alone by Chapman et al. (2005), who overestimate these quantities by 13% and a factor of $\simeq 2$, respectively, when assuming the local far-infrared to radio correlation. This discrepancy can be fully reconciled if a different constant of correlation is assumed for SMGs (see Section 4).

We confirm that the SMG population is dominated by extremely luminous (several times $10^{12} L_\odot$) systems with $\simeq 10^9 M_\odot$ of heated dust, and characteristic 35 K dust temperatures typical to actively star forming ULIRGs. As anticipated, these objects resemble the nearby archetypal ULIRG, Arp 220 (with $T_d \approx 37 \text{ K}$, similarly obtained), except that they are about 7 times more luminous on average.

3.1. Cold, Quiescent SMGs?

In addition, there appear to be several cooler ($T_d \lesssim 25 \text{ K}$), less luminous (10^{11} – $10^{12} L_\odot$) objects, albeit with comparable dust masses (few times $10^9 M_\odot$) present in the population (sources 14 and 19, and possibly 3, 9, and 10 in Tables 2 and 3). While these resemble the Milky Way in temperatures, and hence probably in star formation densities, they are tens of times more luminous than the Galaxy.

This combination of extreme dust masses yet surprisingly low relative star formation rates, indicated by the lesser dust heating, allude to possibly incorrect low-redshift identifications. Should these galaxies lie at the higher, more typical redshifts of the SMG population, their temperatures and luminosities would closely resemble those of the hotter population. However, while lensing of distant SMGs by massive foreground galaxies at the measured redshifts, is conceivable (Blain et al. 1999a; Chapman et al. 2002), these should be rare, and unlikely to account for all cold SMGs.

Alternatively, these seemingly normal type galaxies could, potentially, be remnants to the more remote, hotter pop-

⁷ The CO fluxes from Tacconi et al. (2006) were converted into gas masses using the conversion factor X_{CO} of $0.8 M_\odot (\text{K km s}^{-1} \text{ pc}^2)^{-1}$ in Solomon et al. (1997) appropriate for ULIRGs (Downes & Solomon 1998). The results are therefore consistent with Greve et al. (2005).

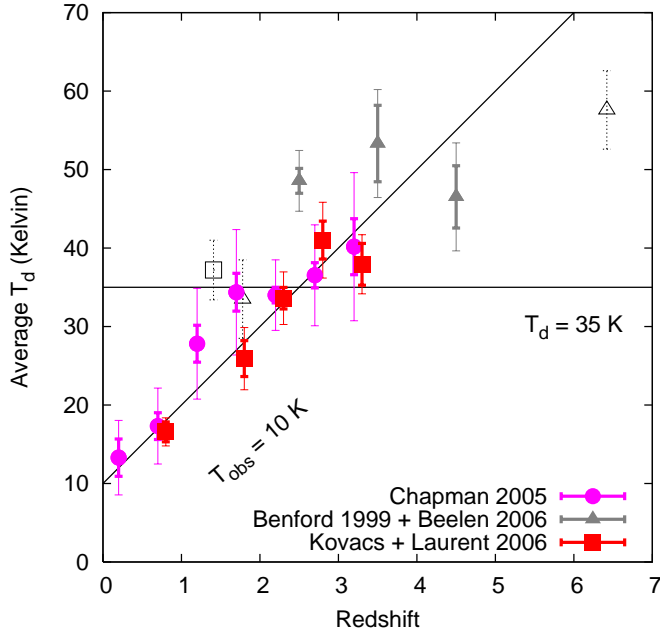


FIG. 4.— Median dust temperatures vs. redshift. Data are binned for this paper (*squares*), for the Chapman et al. (2005) sample (*circles*) with temperature estimates incorporating the radio data, and for dusty quasars (*triangles*). One-sigma error bars were estimated from the scatter inside the bins and the uncertainties of dust temperatures where available (*thick bars*). Dispersion within bins are also shown (*thin bars*), while dotted error bars indicate measurement error for single datum inside a bin. A T_d of 35 ± 3 K may be applicable for $z \sim 1.5$ – 3.5 , which, if true, can provide photometric redshifts in that range. However, observing frame temperatures of around 10 K appear to fit the SMG data somewhat better than constant T_d in the rest frame. This similarity of the SEDs in the observing frame may owe to selection effects.

ulation of SMGs, once the short lived starbursting activity subsides. Dust could persist and remain detectable in the more proximate universe, provided that radiation from the rapidly growing black holes (Borys et al. 2005; Alexander et al. 2005a) does not disperse dust entirely, e.g. dusty QSOs of Benford et al. (1999) and Beelen et al. (2006), or if the dust can later reassemble to form large disk galaxies, like source 14, which is consistent with the large spiral disk galaxy seen in *Hubble Space Telescope* images (Almaini et al. 2006; Borys et al. 2006), or the cold dust mergers suggested by the chain of $16 \mu\text{m}$ emission seen for source 19. This connection between the hot and cold SMGs is further hinted at by the apparent trend of dust temperatures increasing with redshift (Fig. 4) even without the low-redshift data. We, therefore, find the existence of massive cold SMGs plausible.

4. THE FAR-IR/RADIO CORRELATION AT HIGH REDSHIFTS

One of the most valuable uses of the new measurements is to test the local far-infrared to radio correlation at the redshifts of SMGs ($z \sim 1$ – 3). The simple extension of the correlation into the distant universe was suggested by earlier studies based on a combination of 1.4 GHz radio with *Infrared Space Observatory* (ISO) $15 \mu\text{m}$ (Garrett 2002) and *Spitzer* 24 and $70 \mu\text{m}$ observations (Appleton et al. 2004), both of which take advantage of SED template fitting to extrapolate fluxes into the far-infrared regime. More recently, Beelen et al. (2006) hints at the validity of the correlation in the case of a handful of distant ($z \sim 2$ – 6) quasars with SEDs well constrained directly from far-infrared measurements.

A quantitative treatment of the correlation (Helou et al. 1985) has been formulated in terms of the *Infrared Astronomical Satellite* (IRAS) 60 and $100 \mu\text{m}$ fluxes, expressed in the

rest frame as

$$q = \log \left(\frac{\text{FIR}}{3.75 \times 10^{12} \text{ W m}^{-2}} \right) - \log \left(\frac{S_{1.4\text{GHz}}}{\text{W m}^{-2} \text{ Hz}^{-1}} \right), \quad (5)$$

where the far-infrared parameter $\text{FIR} = 1.26 \times 10^{-14} (2.58 S_{60\mu\text{m}} + S_{100\mu\text{m}}) \text{ W m}^{-2}$ and the fluxes $S_{60\mu\text{m}}$ and $S_{100\mu\text{m}}$ are in Jy. The quantity essentially estimates the flux in a wide band centered at $80 \mu\text{m}$ and is a good tracer of the far-infrared luminosity for temperatures in the range of 20–80 K and emissivity indices $\beta \sim 0$ – 2 (Helou et al. 1988).

Perhaps a better measure of the correlation is obtained by directly comparing luminosities. Therefore, we propose to use

$$q_L = \log \left(\frac{L_{\text{FIR}}}{[4.52 \text{ THz}] L_{1.4\text{GHz}}} \right). \quad (6)$$

Here the normalization frequency 4.52 THz has been derived for the adopted greybody model⁸ such that $q_L \rightarrow q$ for $T = 40$ K and $\beta = 1.5$, thus approximating the original definition of q while extending its usefulness beyond the original restrictions in temperature and emissivity. Radio luminosities, in turn, are calculated as

$$L_{1.4\text{GHz}} = 4\pi D_L^2 S_{1.4\text{GHz}} (1+z)^{\alpha-1}, \quad (7)$$

which includes a bandwidth compression by $(1+z)^{-1}$ and a K -correction $(1+z)^\alpha$ to rest frame 1.4 GHz. We assume a synchrotron power law of $S \propto \nu^{-\alpha}$, with the spectral index α for which a typical value of 0.7 (Condon 1992) of nonthermal radio sources is assumed for the calculations.⁹

We confirm that the far-infrared to radio correlation appears to hold throughout the redshift range of $z \sim 1$ – 3 (Figs. 5 and 6), with the notable exceptions of sources 9 and 10, which likely host radio loud AGNs¹⁰. The detections reveal $\bar{q} \approx 2.07 \pm 0.09$ and $\bar{q}_L = 2.12 \pm 0.07$ with intrinsic spreads estimated at $\sigma_q \approx 0.21$ and $\sigma_{q_L} \approx 0.12$ around the respective mean values. The alternative radio fluxes of Biggs & Ivison (2006) provide q values that are higher by 0.06 on average and scatter slightly more with $\sigma_q \approx 0.30$ and $\sigma_{q_L} \approx 0.23$.

The reduced dispersion in q_L vs. q and the somewhat peculiar case of the two cold lower redshift objects (14 and 19), whose derived dust temperature of only 16 K fall outside the range where FIR traces luminosity (eq. [5]) highlight the practicality of the luminosity-based q_L -measure over the original IRAS-based q . The derived mean values are significantly less than the locally observed median values of 2.75 ± 0.03 for local spirals and starbusts galaxies from the IRAS Faint Source Catalog (Condon & Broderick 1991), 2.34 ± 0.01 for radio-identified, flux-limited ($S_{60\mu\text{m}} > 2$ Jy) IRAS sources (Yun et al. 2001), or $\simeq 2.3$ for a range of normal galaxies (Condon 1992) that include spirals and irregulars, E/S0 types, IRAS and radio-selected samples. The corresponding local scatters are also larger, with $\sigma_q = 0.14$, $\sigma_q = 0.33$, and $\sigma_q \lesssim 0.2$, respectively.

Moreover, we find the relationship to be linear, within measurement uncertainty, over nearly three decades of luminosities of the observed SMGs, with a best-fit FIR to radio luminosity index, $d \log L_{\text{FIR}} / d \log L_{1.4\text{GHz}}$, of 1.02 ± 0.12 .

⁸ If SEDs include power law Wien tails instead, the normalizing frequency should be appropriately scaled by $\eta_\beta(\alpha)$. Similar adjustments to the normalization can be derived for any other SED model, hence the shape of the particular SED model used has no effect on the correlation parameter q_L otherwise

⁹ The assumption of the radio spectral index α is not critical. Indices different by $\delta\alpha$ may produce a small bias in q on the order of $\delta q \approx 0.5\delta\alpha$ in the redshift range of $z \sim 1$ – 3 of SMGs, with an undetectable redshift dependence as $\delta q \ll \sigma_q$.

¹⁰ Source 9 has been characterised as an AGN by Chapman et al. (2005)

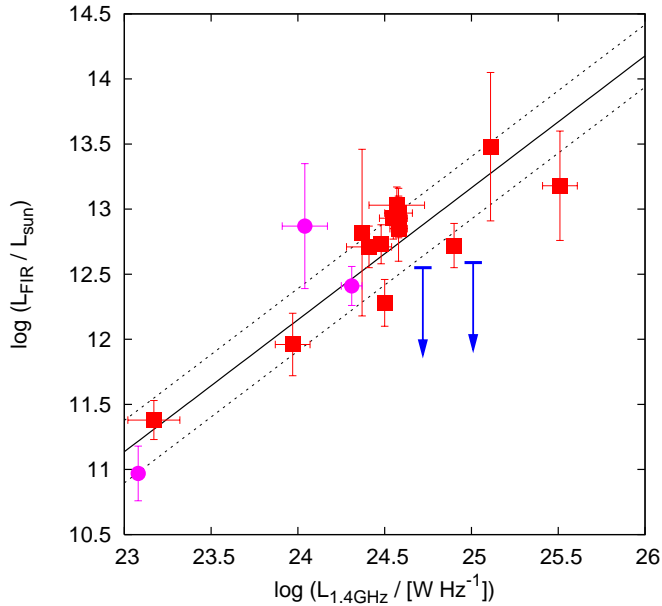


FIG. 5.— Radio to far-infrared correlation for SMGs. Galaxies observed by the authors shown with squares, data from Laurent et al. (2006) with circles. Two-sigma upper limits are indicated when appropriate (arrows). Far-infrared luminosities were calculated exclusively based on the available submillimeter measurements, with $\beta = 1.5$. The best-fit model (solid line) reveals no deviation from linearity in the relationship. The deduced 2σ intrinsic scatters around the model are also shown (dotted lines).

Nonetheless, small levels of nonlinearity, like those discussed by Fitt et al. (1988); Cox et al. (1988); Devereux & Eales (1989) and Condon et al. (1991) remain possible.

The low q -values, the tightness of the correlation, the observed linearity, and the typically warm dust temperatures all point to dust heating that is dominated by high-mass ($> 8 M_{\odot}$) stars. In the two-component model of Yun et al. (2001), short-lived ($< 10^7$ yr) high-mass stars fuel the “hot” thermal component that is strongly coupled to the nonthermal radio via Type II supernovae, whereas the “cold” component heated by a different population of lower mass stars is expected to produce a different correlation with a weaker coupling. They estimate $q_1 = 2.3$ and $q_2 > 4$ for the components. As most galaxies contain both components, intermediate q -values are typically observed. The low q ’s that characterize SMGs are, therefore, indicative of the predominance of high-mass star formation in the dust heating. Moreover, the SMG result forces the revision of the “hot” component correlation to $q_1 \lesssim 2.1$, or lower still (by about 0.16), if steeper radio spectral slopes of $\alpha \simeq 1$ are assumed for these very luminous objects (Yun et al. 2001).

The presence of radio-quiet AGNs would contribute to the total far-infrared emission, biasing towards higher values of q . Radio-loud AGNs, on the other hand, would produce low q -values, albeit to wildly varying extent, which should manifest as an increased spread in the correlation. The tightness of the observed correlation, therefore, confirms that radio-loud AGNs are rare, while the low q -values, otherwise observed, indicate that the AGN contribution to the far-infrared luminosity is small when compared to heating from star formation activity in SMGs. This is consistent with Alexander et al. (2005a,b), who used ultra-deep *Chandra* X-ray data to find that the AGNs, present in at least 75% of SMGs, contribute little to the total bolometric luminosity of their hosts. Dust heating, therefore, is assumed to be star-formation-dominated.

Last but not least, the low q -values observed may partially arise from selection bias, as our initial sample would

miss SMGs with low radio fluxes, i.e., sources with higher q -values, in the secondary selection required for redshift identification. However, faint radio sources with undetectable submillimeter counterparts, representing a hypothesized hot extension to the SMG population, may be more typical (Chapman et al. 2004; Blain et al. 2004), and thus selection bias could be reversed, missing the low q -values instead.

5. DUST EMISSIVITY INDEX

It is possible to further constrain the dust properties, e.g. by measuring the effective emissivity index β . In principle, this may be attempted on an individual basis, since several galaxies have MAMBO (Greve et al. 2004) and/or Bolocam (Laurent et al. 2005) detections at longer wavelengths, providing justification for a three-parameter fit. In practice, however, such an approach is unlikely to yield robust quantities for individual galaxies (see Fig. 2) owing to the proximity of the observed bands and the modest significance of the detections. Therefore, we aimed to fit a single emissivity slope β for the entire sample, hoping to provide a better constrained, ensemble-averaged, dust emissivity index. Moreover, we extend our sample to Chapman et al. (2005) SMGs with multiband submillimeter data that were not observed in this paper. MAMBO associations (Greve et al. 2004) and the 350 μm follow-up of Bolocam and candidates (Laurent et al. 2006) provide five extra sources.

We analyse the data consisting of detections only separately from the data including measurement peaks inside the search area for nondetections. While the first set may appear more robust, it could be more susceptible to selection biases due to the rigorous detection requirement. The larger set, containing upper limits, is thus likely to be less biased of the two and could provide a better characterisation of the whole SMG population.

We have used a modified, nested version of the downhill simplex method (Press et al. 1986) to perform the fit, yielding $\beta = 2.42 \pm 0.71$, a value that is too uncertain to distinguish between the expected values in the range of 1–2. However, the demonstrated validity of the linear far-infrared to radio correlation for the SMG sample allows us to incorporate the radio fluxes to constrain the total integrated far-infrared luminosities and improve the quality of the fit. Here we assumed 0.12 dex as the intrinsic spread in q_L , producing the expected model deviation with $\chi^2 \rightarrow 1$, and consistent with the scatter observed for local spirals and starbursts (Condon et al. 1991).

To avoid radio-loud objects biasing our analysis, we ignored sources 9 and 10 due to their a priori low q_L -values. At the same time, we utilized a modified χ deviation definition to allow some of the sources to become “radio-loud” in the fit, i.e. to significantly deviate from the correlation in the lower q_L direction. Specifically, when the derived q_L value for a source is more than 2σ below the average \bar{q}_L of the fit, we use a relaxed deviation with $\sigma'_{q_L} = 2$, more characteristic of radio loud objects, while keeping χ^2 continuous over the entire parameter space. The fraction of normal sources falsely identified as “radio-loud” by this method is expected to be around 2%, and therefore the effects of mischaracterizations are expected to remain limited.

With the local median q value of 2.34 we obtain $\beta = 0.81 \pm 0.19$ for the detections and $\beta = 1.00 \pm 0.19$ when all the available information is used in the analysis. Both these results imply an emissivity index significantly less than the usually quoted values around 1.5. The interpretation, however, relies entirely on the assumption that the local radio-far-infrared

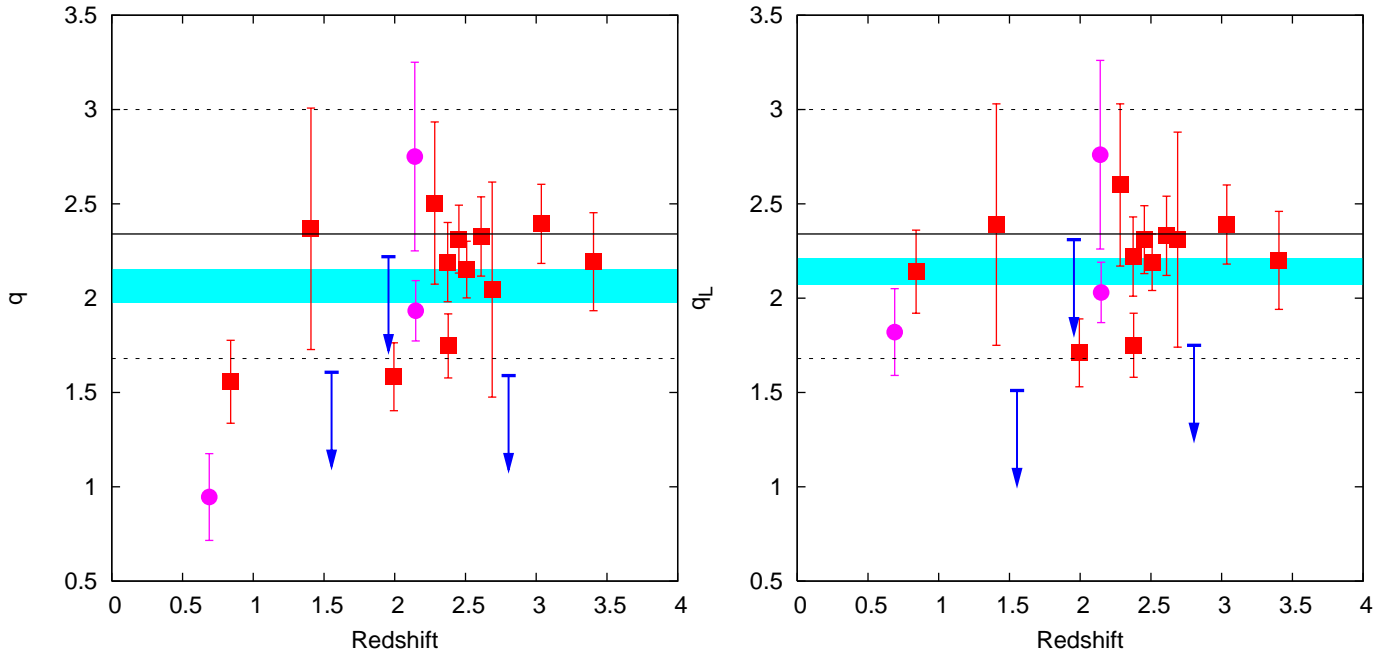


FIG. 6.— (a) Original definition of q from Helou et al. (1985), and (b) the modified, luminosity-based definition q_L as a function of redshift. Two-sigma upper limits are indicated as appropriate (arrows). Data from this paper are shown with squares, while those from Laurent et al. (2006) are shown as dots. The observed SMG’s seem to consistently fall below the locally observed mean of 2.34 (Yun et al. 2001) for local bright *IRAS* sources (solid line) whose 2σ scatters are also indicated (dashed lines). The values were all derived assuming $\beta = 1.5$. The derived distribution mean values of the non-radio-loud subsample ($q > 1$) are also shown (shaded bands).

correlation holds unaltered for higher redshifts.

For a more rigorous treatment, we obtained confidence contours for the likely combinations of both β and q_L (Fig. 7), hence avoiding a priori assumptions on both of these quantities. The smaller set, with detection requirement imposed, favours somewhat lower β -values, in combination with “normal” q_L , with the best fit located at the respective values of 0.95 and 2.27, whereas the more inclusive data set tends towards emissivity indices in line with expectations, but with q_L decidedly below the mean in the local universe. The best-fit values of the extended set are at $\beta = 1.63$ and $q_L = 2.10$. Accordingly, we assumed $\beta = 1.5$ and used the corresponding $q_L = 2.14$ (from Fig. 7) to calculate most likely estimates of the far-infrared emission properties, which are listed in Table 3.

Systematic biases in the cross-calibration, between the SHARC-2 and the longer wavelength data points, would introduce bias into the estimated emissivity index. Fortunately, with expected 10% relative calibration error, the resulting bias is only $\delta\beta \simeq 0.08$, and our conclusions on the dust emissivity are nearly unaffected.

6. PHOTOMETRIC REDSHIFTS

Obtaining accurate redshifts for distant SMGs has relied on optical measurements, guided by radio or optical associations (Chapman et al. 2003, 2005). This approach has been very successful, providing accurate redshifts for nearly a hundred SMGs to date, but it is unlikely to be practical for compiling much larger samples. Moreover, the identifications involving radio or optical counterparts could introduce selection biases into the samples. For both reasons a “holy grail” of large submillimeter surveys has been to obtain redshifts directly from the radio, submillimeter, and mid- to far-infrared (e.g. *Spitzer*) if possible.

The simplest types of redshift estimators, such as Carilli & Yun (1999, 2000a,b), Wiklind (2003) and Laurent et al. (2006), assume that all SMGs have intrin-

sically similar rest-frame temperatures. In essence, redshifts are calculated as $(1+z) \approx T_d/T_{\text{obs}}$ (Blain 1999) for SEDs characterized by T_{obs} in the observing frame and an assumed representative dust temperature T_d for all objects. The methods only differ in how T_{obs} is estimated from the various available flux data. Only independent, and accurate,

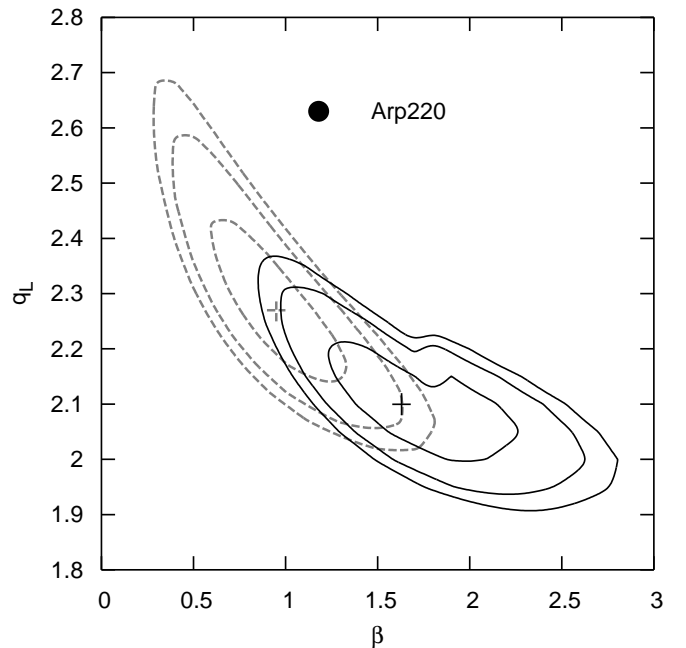


FIG. 7.— Likelihood contours (at 68%, 90%, and 95% confidence) for the dust emissivity β and the radio to far-infrared correlation constant q_L , using only the available detections (dashed curves) and all information, including nondetections (solid curves). The best-fit loci of both fits are indicated by crosses. The more inclusive set is expected to be a more reliable indicator of SMG properties, as it is less affected by the selection biases that are introduced by requiring detections in all bands. A similar fit to Arp 220 is also indicated (black dot).

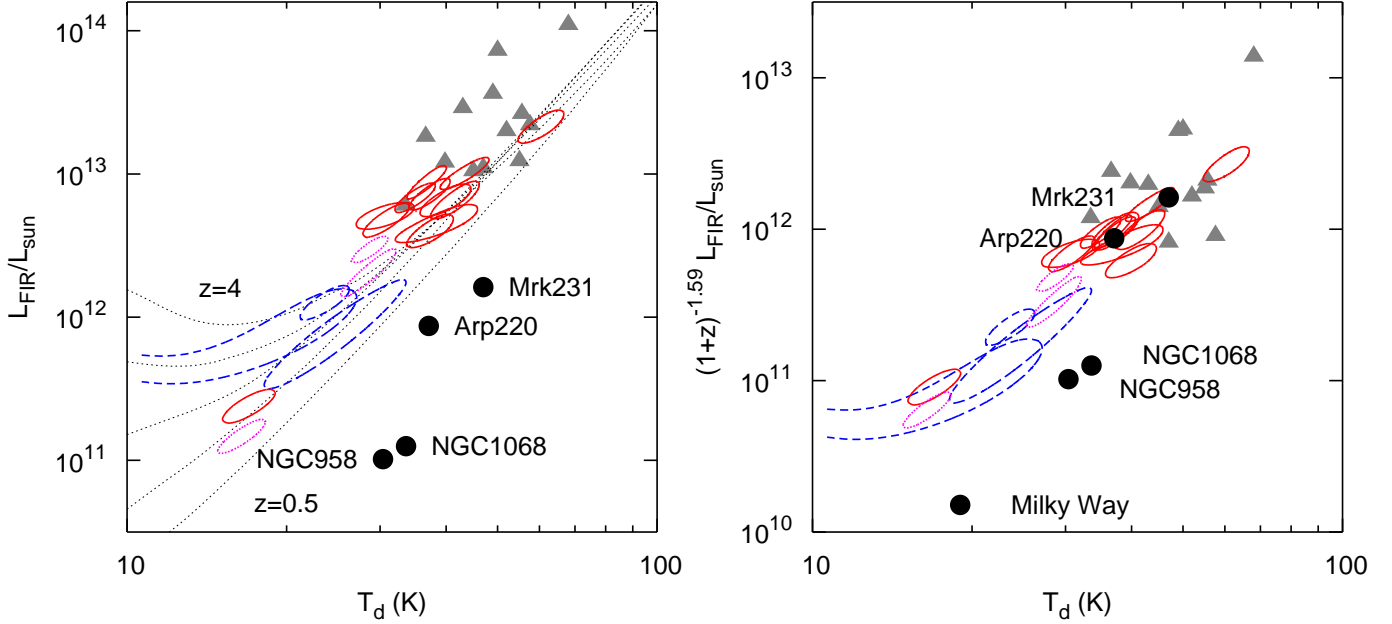


FIG. 8.— Luminosity-temperature (L - T) relation. One-sigma likelihood contours for greybody models fitted to submillimeter data (this paper with solid curves, Laurent et al. [2006] as dotted curves). Contours are also shown for objects not detected by SHARC-2 (*dashed*). The dusty quasars (*triangles*) of Benford et al. (1999) and Beelen et al. (2006), and some well-known objects with accurately constrained SEDs are also shown. The plot highlights the difficulty of measuring the underlying temperature dependence of luminosity, as the two parameters are correlated; most data points are heavily clustered and clearly affected by selection effects. When such a relation is established, however, it can disprove the idea of luminosity-based photometric redshifts. The top graph shows the apparent L - T relation and the 850 μm selection functions ($S_{850 \mu\text{m}} > 5 \text{ mJy}$) at redshifts of 0.5, 1, 2, 3, and 4. (a) The observed relation is evidently biased by selection. (b) A bias- and evolution-free version shows the same relation after the observed redshift evolution (including selection bias) has been accounted for, effectively “moving” luminosities into the present era. The case of nearby Arp 220 clearly supports the case of explicit redshift evolution of the L - T relationship.

measurements of actual dust temperatures for SMGs with known redshifts can test the validity of this approach. We offer this test for the first time.

A glance at Tables 2 and 3 reveals that dust temperatures are distributed around 35 K, with some 80% of the data between 25–45 K. The same conclusion is suggested by the larger Chapman et al. (2005) sample, with the dust temperatures estimated from the SCUBA 850 μm and radio data using the appropriate far-infrared to radio correlation as discussed above. This majority population of SMGs is consistent, within measurement uncertainty, with a single representative temperature of $34.6 \pm 1.4 \text{ K}$ in the rest frame, with an estimated 3 K intrinsic dispersion around the mean, lending some credibility to photometric redshifts derived as

$$(1+z) \approx \frac{(34.6 \pm 3.0) \text{ K}}{T_{\text{obs}}} \left(\frac{1.5}{\beta} \right)^{0.71}$$

in the redshift the range of $z \sim 1.5$ –3.5. However, the observations suggest that these photometric redshift indicators could be wholly inappropriate for as many as 20% of all SMGs, unless some of these outliers have incorrect redshifts. Curiously, the very low q_L -values measured for sources 14 and 19 hint at “hot” type galaxies (Yun et al. 2001), in apparent contradiction with the cool dust temperatures that are implicated at their low redshifts. This mismatch would be reconciled if the temperatures were typical at the photometric z -values of $2.96^{+0.51}_{-0.43}$ and $1.95^{+0.33}_{-0.28}$, respectively.

While quasars (Benford et al. 1999; Beelen et al. 2006) too can be characterised by rest-frame SED templates, with $T_d \approx 48 \pm 8 \text{ K}$ ¹¹ more or less uniformly across $z \sim 2$ –7, they are typically hotter than SMGs, perhaps due to additional dust heating by an AGN. However, quasars, selected from larger

volumes than SMGs, could provide the rare extension of the SMG population into ever more extreme luminosities and hotter dust temperatures. If true, the different temperatures that characterize quasars versus the bulk of SMGs invalidates the single representative temperature assumption for all SMGs, already under fire from a minority population of cold SMGs, and therefore may oppose rather than support the applicability of temperature-based photometric redshifts.

Alternatively, the *entire* SMGs sample, including the low-redshift data, is better fit by temperature evolution of $T_d \propto (1+z)$, producing similar temperatures in the observed frame ($T_{\text{obs}} \simeq 10 \text{ K}$), with an average deviation of $|\hat{\chi}| = 1.40$ versus 2.67 produced by the representative rest-frame temperature model when assuming a 10% intrinsic scatter in T_d . Hence, the temperature range that fits most SMGs could arise from the similar fractional dispersion of the redshift distribution, i.e., objects selected near the median redshift of 2.3 tend to have temperatures of about 35 K. Thus, temperature-based photometric redshifts may not provide additional information beyond a reflection of the median z of the sample.

A similarity of SEDs in the observed frame, yielding a nearly constant T_{obs} and thus $T_d \sim (1+z)$, could arise simply from selection effects that result from the minimum flux requirement for detections (Fig. 8), and the small dynamic range (of a factor $\simeq 3$) of flux densities that characterise current SMG samples. As such, selection effects alone could render far-infrared and radio based photometric redshift indicators wholly unsuitable for unbiased flux- and volume-limited samples of SMGs.

6.1. Luminosity-Temperature Relation

An alternative, luminosity-based approach exploits the hypothetical relationship between dust temperatures and the luminosities that they fuel, to derive photometric redshifts by comparing the rest-frame relationship to observed tem-

¹¹ Temperatures from Beelen et al. (2006) were adjusted for $\beta = 1.5$ for consistency.

perature indicators and fluxes. Like other scaling relations that characterize galaxies, the L - T relationship would, presumably, be a genuine property of galaxies, reflecting the physics of galactic structure and dynamics. While the idea has been drafted by Yun & Carilli (2002), Blain et al. (2003), and Aretxaga et al. (2005), the particular implementation of such a method was left awaiting the determination of the actual form of such an L - T relation.

We find that the far-infrared luminosity is well approximated by a power law of the form

$$L_{\text{FIR}} = \mathcal{L}_0 T_d^\gamma \times (1+z)^\mu \quad (8)$$

for some exponents γ and μ . The expression incorporates the possibility of explicit redshift evolution, approximated by the term $(1+z)^\mu$ chosen for convenience. This independent redshift term is expected to absorb selection effects and allow the determination of the underlying temperature dependence.

The possible combinations of L_{FIR} and T_d pairs are correlated (Fig. 8), which adds difficulty to constraining the underlying relationship. With this warning in mind, our best estimates of the exponents are $\gamma = 2.76 \pm 0.29$ and $\mu = 1.74 \pm 0.38$ for all data points and $\gamma = 2.61 \pm 0.30$ with $\mu = 1.25 \pm 0.48$ excluding the lower redshift points. The corresponding normalizations, \mathcal{L}_0 , are $3.4 \times 10^7 L_\odot$ (± 0.33 dex) and $1.1 \times 10^8 L_\odot$ (± 0.45 dex), respectively. The fits were obtained via a two-variable linear regression of the logarithms with error bars (Table 3) on both the $\log L$ and $\log T$ values. As most galaxies lie in a narrow temperature and luminosity range, we point out that the derived temperature exponents are constrained by relatively few points, some or all of which could be peculiar, and therefore the true uncertainties of γ and μ are likely underestimated. Nonetheless, these scaling models successfully apply to the quasars of Benford et al. (1999) and Beelen et al. (2006), and the local ULIRGs Arp 220 and Mrk 231. If we consolidate our estimates with the inclusion of these objects, we obtain $\gamma = 2.82 \pm 0.29$, $\mu = 1.59 \pm 0.18$, and $\mathcal{L}_0 = 3.6 \times 10^7 L_\odot$ (± 0.46 dex). This relationship, derived for SMGs, quasars, and ULIRGs, could hint at a possible connection among these types of objects; however, it may not apply to the less active galaxies of the local universe (Fig. 8).

Assuming the exponents and scaling are properly determined, we may attempt to derive a photometric redshift indicator by comparing the expressions for the far-infrared luminosity from equations (4) and (8) and from the definitions in equations (6) and (7). In order to facilitate the derivation of analytic solutions, we approximate the luminosity distance by $D_L \approx D_0(1+z)^\delta$, the effect of which is to simplify all redshift dependence to powers of $(1+z)$. This simplification is reasonable for the study of SMGs (leading to an rms $\delta z/z$ of $\simeq 6\%$) in the redshift range of 0.5–4 with $D_0 = 1.63$ Gpc and $\delta = 2.07 \pm 0.03$. We find that the far-infrared luminosity is then proportional to

$$S_{1.4\text{GHz}}(1+z)^{2\delta+1-\alpha} \propto T_{\text{obs}}^\gamma (1+z)^{\gamma+\mu} \propto \frac{S_\nu T_{\text{obs}}^{4+\beta}}{e^{h\nu/kT} - 1} (1+z)^{2\delta}. \quad (9)$$

Substituting the quantities assumed or determined so far, we find that all three expressions possess similar dependences on $(1+z)$, with exponents of 4.44 ± 0.12 , 4.41 ± 0.34 , and 4.14 ± 0.06 , respectively. As the exponents are indistinguishable within the measurement uncertainties involved, we conclude that, in the redshift range of $z \sim 0.5$ –4 of the approximation, it is very unlikely that a meaningful measure of redshift can be deduced in this way—bad news for luminosity-based

photometric redshift estimation. While it may simply be an unfortunate coincidence, it is more likely that the inability to determine redshifts in this manner is, once again, the product of the sample selection yielding candidates with similar observed SEDs. With these being nearly identical in the observing frame, photometric redshifts of any kind remain elusive.

We can, nevertheless, derive a true luminosity-based photometric redshift indicator in the low-redshift limit $z \ll 1$, where the luminosity distance takes the asymptotic form $D_L \rightarrow cz/H_0$. In this limit,

$$z \approx 1 \text{ Gpc} \frac{H_0}{c} \left(\frac{\mathcal{L}_0 T_d^\gamma}{L_{1 \text{ Gpc}}} \right)^{1/2},$$

where $L_{1 \text{ Gpc}}$ is what the luminosity would be if the galaxy were at a distance of 1 Gpc. While this is irrelevant to the SMG sample, it provides a useful expression for the study of the L - T relation in the nearby ($z \ll 1$) universe, when values of z are already known.

Comparing the L - T relationship (eq. [8]) with the expression for the integrated far-infrared luminosity (eq. [4]) we infer that $M_d \propto T_d^{-(4+\beta-\gamma)}(1+z)^\mu$, i.e., at any given redshift $T_d \propto M_d^{1/(4+\beta-\gamma)}$, that is $T_d \propto M_d^{-0.38 \pm 0.04}$, which is expected to be free of selection bias. The dust heating is predominantly fueled by the luminosity of massive ($> 8 M_\odot$) stars, and so we find that the number of high-mass stars $N_{\text{HM}} \propto T_d^\gamma$, assuming that the high-mass IMF and stellar content of all SMGs is similar. We may estimate the high-mass star formation efficiency in SMGs by $\eta_{\text{HM}} \propto N_{\text{HM}}/M_d \propto M_d^{-\gamma/(4+\beta-\gamma)}$; i.e., $\eta_{\text{HM}} \propto M_d^{-1.10 \pm 0.13}$.

Surprisingly, this implies that more dusty galaxies produce, and thus contain, fewer massive stars relative to dust mass. Perhaps this is due to more dusty environments favoring lower mass star formation. This conclusion is consistent with the evolution of q from lower values in SMGs to higher values in nearby dusty disk galaxies (Yun et al. 2001) and with the dominance of high-mass stars in SMGs giving way to more radio-quiet low-mass stars heating dust in the local universe (Blain et al. 1999b; Baugh et al. 2005).

7. SCALING RELATIONS

After cancelling the nearly identical redshift terms appearing in the luminosity scaling relations (eq. [9]), we obtain a useful set of expressions interrelating the observed quantities, $S_{1.4\text{GHz}}$, S_ν and T_{obs} in the far-infrared. For distant SMGs, in the redshift range $z \sim 0.5$ –4, we find

$$S_{1.4\text{GHz}} \propto T_{\text{obs}}^\gamma, \\ S_\nu \propto T_{\text{obs}}^{\gamma-(4+\beta)} \left(e^{h\nu/kT} - 1 \right).$$

The appropriate constants of proportionality are easily derived from the relevant expressions (eqs. [4], [7], [6] and [8]) applied at the median redshift of the sample. Figure 9 testifies to the predictive power of these relations. Excluding the radio-loud points, which clearly lie away from the far-infrared to radio correlation, the model is consistent with observations within the measurement uncertainties. We emphasize, that these relations are not fitted to the data, but rather a direct consequence of the radio to far-infrared correlation, and the deduced L - T relation.¹² Therefore, the excellent agreement with data is remarkable.

¹² A pure L - T relation without the evolution term yields a poor model of the observed relations which therefore directly support the inclusion of the explicit redshift evolution in eq. (8).

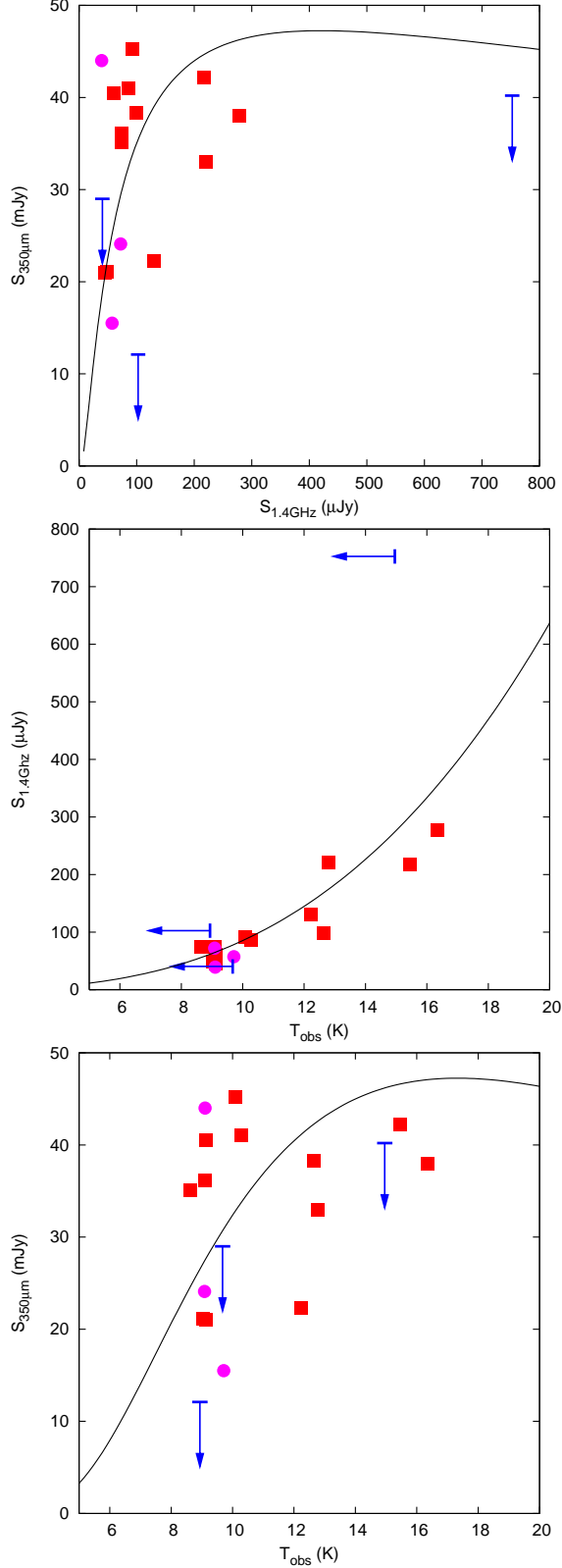


FIG. 9. — Relations between observed quantities. (a) Radio and far-infrared fluxes, (b) radio fluxes, and (c) far-infrared fluxes vs. observed temperatures. Results from this paper are plotted as squares with upper limits indicated as appropriate (arrows), Laurent et al. (2006) data are shown as circles. The model deriving from the radio-FIR correlation and the observed L - T relation is also shown (solid curve). The data show excellent agreement with predictions within the measurement uncertainties involved. A single radio or submillimeter measurement may, therefore, suffice to predict the other quantities. Thus, these relationship can offer a useful tool for all radio or submillimeter surveys.

8. CONCLUSIONS

New 350 μm data lead to the first direct measures of the characteristic dust temperatures and far-infrared luminosities of SMGs and the following valuable conclusions.

1. The linear radio to far-infrared correlation remains valid out to redshifts of $z \sim 1-3$ for SMGs, with the exception of rare radio-loud objects. The power-law index in the correlation is 1.02 ± 0.12 , and tighter than observed locally, with an intrinsic dispersion of only 0.12 dex.
2. Either the far-infrared-radio correlation constant q is lower than locally measured ($q_L \approx 2.14 \pm 0.07$) or the effective dust emissivity index is less, with $\beta \rightarrow 1$ consistent with observations. The lower q -value indicates that dust heating is dominated by high-mass stars and that any AGN contribution is minor in comparison.
3. Compared with low-redshift galaxies, SMGs are characterized either by low gas-to-dust ratios, around $54^{+14}_{-11} (\kappa_{850\mu\text{m}}/0.15 \text{ m}^2 \text{ kg}^{-1})$, indicating dust-rich environments, or by efficient dust absorption of $\kappa_{850\mu\text{m}} \gtrsim 0.33 \text{ m}^2 \text{ kg}^{-1}$.
4. Far-infrared- and radio-based photometric redshifts might be appropriate for up to 80% of SMGs in the redshift range of $z \sim 1.5-3.5$, with a rest-frame temperature assumption of $34.6 \pm 3.0 \text{ K} (1.5/\beta)^{0.71}$. However, photometric redshift indicators may not be appropriate for an unbiased SMG sample, as existing selection effects tend to favor measuring SEDs that are similar in the observed frame.
5. We deduce an L - T relationship that we argue to be a property of star-forming galaxies. When recast as mass scaling, we find, that ISM heating scales inversely with the quantity of dust in the galaxies i.e., the galaxies with more dust are less active, possibly due to the formation of more low-mass stars being favoured in dustier environments.
6. From the observed L - T relation, possibly biased by selection, and the radio to far-infrared correlation, we derive scaling relations among the observed quantities $S_{1.4\text{GHz}}$, S_ν in the submillimeter or far-infrared, and the observing frame dust temperature T_{obs} , applicable to the redshift range of $z \sim 0.5-4$. A determination of one of these quantities may sufficiently characterise the observed far-infrared properties of SMGs.

The authors wish to thank Sophia Khan, Rick Shafer, and Min Yang for their help with collecting data debugging CRUSH; Jonathan Bird for his contributions to the calibration and observing; Thomas Greve and Harvey Moseley for discussions and helpful insights regarding interpretation; Melanie Leong for her efforts to shorten observing times through improvements to the dish surface, Hiroshige Yoshida for all-around software support at the CSO; and the referee for improving this paper through thoughtful comments. We would further like to express our gratitude for the generous sponsorship of the National Science Foundation in funding this research.

Facilities: CSO (SHARC-2)

REFERENCES

- Agladze, N. I., Sievers, A. J., Jones, S. A., Burlitch, J. M., & Beckwith, S. V. 1996, *ApJ*, 462, 1026
- Alexander, D. M., Bauer, F. E., Chapman, S. C., Smail, I., Blain, A. W., Brandt, W. N., & Ivison, R. J. 2005a, *ApJ*, 632, 736
- Alexander, D. M., Smail, I., Bauer, F. E., Chapman, S. C., Blain, A. W., Brandt, W. N., & Ivison, R. J. 2005b, *Nature*, 434, 738
- Almaini, O., Dunlop, J. S., Conselice, C. J., Targett, T. A., & Mclure, R. J. 2006, *MNRAS*, submitted
- Appleton, P. N., et al. 2004, *ApJS*, 154, 147
- Aretxaga, I., Hughes, D. H., & Dunlop, J. S. 2005, *MNRAS*, 358, 1240
- Barger, A. J., Cowie, L. L., Sanders, D. B., Fulton, E., Taniguchi, Y., Sato, Y., Kawara, K., & Okuda, H. 1998, *Nature*, 394, 248
- Baugh, C. M., Lacey, C. G., Frenk, C. S., Granato, G. L., Silva, L., Bressan, A., Benson, A. J., & Cole, S. 2005, *MNRAS*, 356, 1191
- Beelen, A., Cox, P., Benford, D. J., Dowell, C. D., Kovács, A., Bertoldi, F., & Omont, A. 2006, *ApJ*, 642, 694
- Benford, D. J., Cox, P., Omont, A., Phillips, T. G., & McMahon, R. G. 1999, *ApJ*, 518, L65
- Biggs, A. D., Ivison, R. J. 2006, *MNRAS* 371, 963
- Blain, A. W. 1999, *MNRAS*, 309, 955
- Blain, A. W., Barnard, V., & Chapman, S. C. 2003, *MNRAS*, 338, 733
- Blain, A. W., Chapman, S. C., Smail, I., & Ivison, R. J. 2004, *ApJ*, 611, 52
- Blain, A. W., Möller, O., & Maller, A. M. 1999a, *MNRAS*, 303, 423
- Blain, A. W., Smail, I., Ivison, R. J., & Kneib J.-P. 1999b, *MNRAS*, 302, 632
- Borys, C., Chapman, S., Halpern, M., & Scott, D. 2003, *MNRAS*, 344, 358
- Borys, C., Smail, I., Chapman, S. C., Blain, A. W., Alexander, D. M., & Ivison, R. J. 2005, *ApJ*, 635, 853
- Borys, C., et al. 2006, *ApJ*, 636, 134
- Carilli, C. L., & Yun, M. S. 1999, *ApJ*, 513, L13
- Carilli, C. L., & Yun, M. S. 2000a, *ApJ*, 530, 618
- Carilli, C. L., & Yun, M. S. 2000b, *ApJ*, 539, 1024
- Chapman, S. C., Blain, A. W., Ivison, R. J., & Smail, I. 2003, *Nature*, 422, 695
- Chapman, S. C., Blain, A. W., Smail, I., & Ivison, R. J. 2005, *ApJ*, 622, 772
- Chapman, S. C., Smail, I., Blain, A. W., & Ivison, R. J. 2004, *ApJ*, 614, 671
- Chapman, S. C., Smail, I., Ivison, R. J., & Blain, A. W. 2002, *MNRAS*, 335, L17
- Condon, J. J. 1992, *ARA&A*, 30, 575
- Condon, J. J., Anderson, M. L., & Helou, G. 1991, *ApJ*, 376, 95
- Condon, J. J., & Broderick, J. J. 1991, *AJ*, 102, 1663
- Coppin, K., Halpern, M., Scott, D., Borys, C., & Chapman, S. 2005, *MNRAS*, 357, 1022
- Cox, M. J., Eales, S. A. E., Alexander, P., & Fitt, A. J. 1988, *MNRAS*, 235, 1227
- De Breuck, C., et al. 2003, *A&A*, 401, 911
- Devereux, N. A., & Eales, S. A. 1989, *ApJ*, 340, 708
- Dowell, C. D., et al. 2003, *Proc. SPIE*, 4855, 73
- Downes, D., & Solomon, P. M. 1998, *ApJ*, 507, 615
- Dunne, L., & Eales, S. A. 2001, *MNRAS*, 327, 697
- Dunne, L., Eales, S. A., & Edmunds, M. G. 2003, *MNRAS*, 341, 589
- Dupac, X., et al. 2003, *A&A*, 404, L11
- Eales, S., Lilly, S., Gear, W., Dunne, L., Bond, R. J., Hammer, F., Le Fèvre, O., & Crampton, D. 1999, *ApJ*, 515, 518
- Fitt, A. J., Alexander, P., & Cox, M. J. 1988, *MNRAS*, 233, 907
- Garrett, M. A. 2002, *A&A*, 384, L19
- Greve, T. R., Ivison, R. J., Bertoldi, F., Stevens, J. A., Dunlop, J. S., Lutz, D., & Carilli, C. L. 2004, *MNRAS*, 354, 779
- Greve, T. R., et al. 2005, *MNRAS*, 359, 1165
- Helou, G., Khan, I. R., Malek, L., & Boehmer, L. 1988, *ApJS*, 68, 151
- Helou, G., Soifer, T., & Rowan-Robinson, M. 1985, *ApJ*, 298, L7
- Hughes, D. H., et al. 1998, *Nature*, 394, 241
- Ivison, R. J., et al. 2002, *MNRAS*, 337, 1
- Kovács, A. 2006, PhD thesis, California Institute of Technology, <http://etd.caltech.edu/etd/available/etd-06022006-123747>
- Laurent, G. T., Glenn, J., Egami, E., Rieke, G. H., Ivison, R. J., Yun, M. S., Aguirre, J. E., & Maloney, P. R. 2006, *ApJ*, 643, 38
- Laurent, G. T., et al. 2005, *ApJ*, 623, 742
- Leong, M. M. 2005, *URSI Conf. J3-10*, 426, <http://astro.uchicago.edu/ursi-comm-J/ursi2005/rf-telescope-fabrication/leong>
- Press, W. H., Flannery, B. P., & Teukolsky, S. A. 1986, *Numerical Recipes in C: The Art of Scientific Computing* (Cambridge: Cambridge Univ. Press)
- Smail, I., Ivison, R. J., & Blain, A. W. 1997, *ApJ*, 490, L5
- Smail, I., Ivison, R. J., Owen, F. N., Blain, A. W., & Kneib, J.-P. 2000, *ApJ*, 528, 612
- Solomon, P. M., Downes, D., Radford, S. J. E., & Barrett, J. W. 1997, *ApJ*, 478, 144
- Seaquist, E., Yao, L., Dunne, L., & Cameron, H. 2004, *MNRAS*, 349, 1428
- Stevens, J. A., Amure, M., & Gear, W. K. 2005, *MNRAS*, 357, 361
- Tacconi, L. J., et al. 2006, *ApJ*, 640, 228
- Webb, T. M. A., Lilly, S. J., Clements, D. L., Eales, S., Yun, M., Brodwin, M., Dunne, L., & Gear, W. K. 2003, *ApJ*, 597, 680
- Wiklund, T. 2003, *ApJ*, 588, 736
- Yun, M. S., & Carilli, C. L. 2002, *ApJ*, 568, 88
- Yun, M. S., Reddy, N. A., & Condon, J. J. 2001, *ApJ*, 554, 803